J Neurosurg 106:82–89, 2007

Fusion imaging of three-dimensional magnetic resonance cisternograms and angiograms for the assessment of microvascular decompression in patients with hemifacial spasms

Toru Satoh, M.D.,[1] Keisuke Onoda, M.D.,[2] and Isao Date, M.D.[2]

[1]Department of Neurological Surgery, Ryofukai Satoh Neurosurgical Hospital, Fukuyama, Hiroshima; and [2]Department of Neurological Surgery, Okayama University Graduate School of Medicine, Dentistry and Pharmaceutical Sciences, Okayama, Japan

Object. The precise preoperative assessment of the complex nerve–vessel relationship at the root exit zone (RExZ) of the facial nerve is important when planning microvascular decompression (MVD) in patients with hemifacial spasms. The authors have developed an imaging technique—the fusion of 3D magnetic resonance (MR) cisternography and coregistered 3D MR angiography images—that allows clear visualization of the spatial relationship between the vessels and the rootlet of the facial nerve at the brainstem.

Methods. The authors reconstructed 3D MR cisternograms and 3D MR angiograms by using a perspective volume-rendering algorithm that they applied to the volumetric data sets of the following modalities: MR cisternography (a T_2-weighted 3D fast spin echo sequence) and coregistered MR angiography (a 3D time-of-flight sequence). The complex anatomical relationship between the offending vessels and the facial nerve RExZ was inspected preoperatively by examining the fusion images from various perspectives within the cerebellopontine angle cistern, within the affected facial nerve, and through the simulated surgical route. The reconstructed 3D findings of the nerve–vessel relationship were compared with the intraoperative findings. Postoperatively, the fused 3D MR imaging technique was used to confirm that microsurgical dissection and the interposed prosthesis had succeeded in maintaining the causative vessels in a position away from the RExZ.

Conclusions. The fusion of 3D MR cisternograms and 3D MR angiograms may prove useful in the pre- and postoperative assessment of MVD in patients with hemifacial spasm.

Key Words • **neurovascular compression** • **neurovascular contact** • **cranial nerve** • **brainstem** • **magnetic resonance cisternography** • **three-dimensional imaging**

Hemifacial spasm is categorized as a hyperactive cranial nerve dysfunction syndrome, and most instances are caused by aberrant and tortuous arteries producing mechanical compression at the facial nerve RExZ.[7,9,16] Microvascular decompression via a lateral suboccipital approach is widely performed to treat patients with hemifacial spasm.[9,10,19] Recently, MR angiography and MR cisternography have been used to evaluate the anatomy prior to MVD. The pathological arteries compressing the facial nerve at the RExZ can be presumed by studying the source images. In particular, a single MR cisternography image can depict the fine structures of cranial nerves and vessels within the CPA cistern as well as the adjacent brain parenchyma.[2,11–14,17,18,21–25] Because these source images demonstrate the anatomical elements in a 2D fashion, however, it may be difficult to infer the 3D relationship of the nerve–vessel complex at the facial nerve RExZ.

In this study, we used an imaging technique in which 3D MR cisternograms and 3D MR angiograms are fused to provide 3D visualization and allow assessment of MVD in patients with hemifacial spasm. The 3D MR cisternogram represents a reconstructed T_2-weighted 3D FSE sequence, and the 3D MR angiogram is an MR angiogram reconstructed from a 3D TOF SPGR sequence in the steady state. Images of black blood shown on T_2-weighted FSE MR cisternograms and those of bright blood shown on TOF SPGR MR angiograms were coregistered and composed into a single 3D image by using a graphic computer workstation. With a transparent image of the fused 3D MR cisternogram–angiogram, the site of the neurovascular compression was preoperatively assessed three dimensionally from various vantage points in the CPA cistern and within the affected fa-

Abbreviations used in this paper: AICA = anterior inferior cerebellar artery; CPA = cerebellopontine angle; CSF = cerebrospinal fluid; FASE = fast asymmetrical spin echo; FSE = fast spin echo; MR = magnetic resonance; MVD = microvascular decompression; PICA = posterior inferior cerebellar artery; RExZ = root exit zone; SPGR = spoiled-gradient recalled; TOF = time-of-flight; VA = vertebral artery.

cial nerve. The simulated image depicting the surgical route was compared with the intraoperative image showing the spatial relationship between the presumed offending artery and the facial nerve at the rootlet from the brainstem. Postoperatively, a fusion image was made to ensure that the pathological vessels had been safely distanced from the facial nerve RExZ by microsurgical dissection and interposition of a prosthesis. The feasibility and accuracy of the transparent fusion image in the pre- and postoperative assessment of MVD for hemifacial spasm are discussed.

Clinical Material and Methods

Patient Population and Clinical Data

A consecutive series of 12 patients with hemifacial spasm visited our hospital for MVD between November 2004 and November 2005; all were included in this study (Table 1). The patients' ages ranged from 36 to 74 years (mean 54.2 ± 18.9 years [standard deviation]). There were two men and 10 women. The spasm affected the right side of the face in three patients and the left side in nine. All patients underwent preoperative MR cisternography and MR angiography, and MVD was performed via a lateral suboccipital approach while auditory brainstem monitoring was conducted.

Acquisition of MR Cisternography Data

Magnetic resonance cisternography was performed with a clinical MR imager (Signa HiSpeed 1.0 t; General Electric Healthcare); a quadrature-head coil was used and a T_2-weighted 3D FSE sequence was obtained. We used the following parameters: TR 4000 msec; TE 160 msec; number of excitations 1; echo train length 128; bandwidth 15.63 KHz; matrix 256 × 256; section thickness 0.6 mm; section interval 0.6 mm; field of view 16 cm; and total imaging time 803 seconds. Overall, 96 continuous source axial images were acquired. Volumetric data were transferred to an independent workstation with medical visualization software (Zio M900 Quadra; AMIN).

The MR cisternography data were processed into the 3D volume-rendering data set (96 data points) in 9 seconds. The 3D MR cisternogram was rendered from the data set in 11 seconds using a perspective volume-rendering algorithm. On the signal-intensity histogram (arbitrary unit distribution) drawn on the source axial image of the cisternogram, the arteries, veins, and dura mater showed profoundly low signal intensity (50–150); cranial nerves and juxtacisternal brain parenchyma, moderately low signal intensity (250–300); and surrounding CSF, profoundly high signal intensity (500–750). To visualize the margin of the vessels, cranial nerves, and brainstem three dimensionally, we selected the entire hypointense area relative to the CSF from the opacity chart of the signal-intensity distribution by using a function of declining curve. The threshold value of this curve was adjusted according to each individual signal-intensity distribution pattern with a threshold range of 420 to 460 (opacity level 100%) declining to 440 to 480 (opacity level 0%, width 20), and color rendered in blue. The 3D MR cisternogram depicted the spatial expansion of the contours of intracisternal objects in relation to juxtacisternal structures and projected from various viewpoints with a visual angle of 90°.

TABLE 1

Clinical features of 12 patients with hemifacial spasm

Case No.	Age (yrs), Sex	Spasm Side	Offending Vessel	Compressed Site	Result
1	51, M	lt	PICA	anterior	excellent
2	36, F	rt	AICA	posterosuperior	excellent
3	69, F	lt	PICA	anteroinferior	excellent
4	61, F	lt	PICA/VA	inferior	excellent
5	64, F	lt	PICA	anterosuperior	excellent
6	47, F	lt	AICA/vein	anterior	excellent
7	59, F	lt	PICA/VA	anterosuperior	excellent
8	64, M	lt	AICA	anteroinferior	excellent
9	54, F	lt	AICA	anterosuperior	excellent
10	65, F	rt	AICA	anteroinferior	excellent
11	66, F	lt	PICA	anteroinferior	excellent
12	74, F	rt	AICA	anteroinferior	excellent

Acquisition of MR Angiography Data

Magnetic resonance angiography was performed with the same image baseline, and data were obtained using a 3D TOF SPGR sequence. We used the following protocol: TR 35 msec; TE 3.9 to 4.1 msec; number of excitations two; flip angle 20°; matrix 192 × 128; section thickness 1.2 mm; section interval 0.6 mm; field of view 16 cm; no magnetization transfer contrast; zero-fill interpolation processing two times; 120 sections in total (two slabs); overlap of eight sections; and total imaging time 529 seconds. A total of 104 continuous source images were obtained. Following this unenhanced MR angiography session, steady-state contrast-enhanced MR angiography was repeatedly performed after the intravenous administration (via the antecubital vein) of meglumine gadopentate (0.1 mmol/kg Magnevist; Schering Japan Co.).

Source axial volumetric data of unenhanced and contrast agent–enhanced MR angiograms were transferred to the same workstation. Data were interpolated every 0.6 mm and processed into the 3D volume-rendering data set (207 data points). The 3D MR angiogram was rendered with a perspective volume-rendering algorithm by using an increasing curve starting with a threshold of 170 to 180 (0% opacity level) and up to 190 to 200 (100% opacity level, width 20), with a visual angle of 90°, and color rendered in red. Unenhanced 3D MR angiography depicted the spatial architecture of the arteries and large veins, and contrast medium–enhanced 3D MR angiography depicted the vessels including branching arteries, veins, and venous sinuses.

Reconstruction of the 3D MR Cisternograms and 3D MR Angiograms

A fusion image of the 3D MR cisternogram and 3D MR angiogram was reconstructed on a workstation by coregistering the 3D MR cisternogram and its coordinated 3D MR angiogram into a single 3D image; each image was created from each volume-rendering data set. To emphasize the vascular components, we used an MR angiography–weighted fusion image[22,23] by compositing the 3D MR cisternogram (opacity level 15%, in blue) and the 3D MR angiogram (opacity level 100%, in red). Alternatively, we used a boundary 3D MR cisternogram[22,23] and rendered it with a perspective volume-rendering algorithm by using a spiked peak curve with a threshold of 440 to 480 (opacity level

100%, width 20, in blue). The boundary 3D MR cisternogram depicted the boundary of the cisternal structures as a series of rings (opacity level 100%, in blue), so that the underlying 3D MR angiogram (opacity level 100%, in red) could be visualized directly through the spaces between rings.

Using reconstruction parameters of the function curves saved on the workstation, we instantly reproduced standard images of the 3D MR cisternogram, the 3D MR angiogram, and a fusion image of the 3D MR cisternogram–angiogram. Thus, the simulated images of the operative field through similar surgical routes were feasibly reconstructed for the different cases; however, certain adjustments of the threshold range—to refine the contours of the objects—and minor changes in visual projections from different vantage points were needed in individual cases. The total mean time required to produce a fusion image was approximately 30 to 50 seconds per image after scanning.

With a 3D MR cisternogram–angiogram fusion image, the spatial relationship of the nerve–vessel complex was assessed preoperatively from the various vantage points in the CPA cistern and within the affected facial nerve per se. The details seen on the simulated images obtained through the surgical route were compared with the operative findings. Postoperatively, the 3D imaging technique was used to demonstrate the successful dislocation of the causative vessels from the RExZ of the facial nerve performed by the microsurgical dissection and the interposition of a prosthesis.

Results

On the 3D MR cisternograms, the anatomical elements in the CPA cistern, including the nerve–vessel complex at the RExZ of the facial nerve, were depicted simultaneously. The facial and vestibulocochlear nerves were identified separately based on their origin in the internal auditory canal and their course toward the nerve rootlets at the brainstem. The arteries were identified by tracing the vessels to their origin from the VA and the veins to a larger vein and venous sinus. The arteries exhibited profoundly low signal intensity and were distinguishable from the cranial nerves and brain parenchyma, which were of moderately low signal intensity, but they could not usually be differentiated from the veins. In the patient with a recurrent hemifacial spasm (Case 11), a malpositioned prosthesis placed in the previous MVD was clearly not between the facial nerve and the brainstem but in the neighboring cistern. Additionally, the contrast medium–enhanced 3D MR angiogram showed that the arteries exhibited profound hyperintensity and that the veins exhibited moderate hyperintensity; the low signal intensity of these vessels was in strong contrast to the adjacent nerve and brainstem at the RExZ.

With the fused 3D MR cisternography–angiography image, the vascular components depicted on the 3D MR cisternogram can be delineated by referencing the overlapped 3D MR angiogram. The contact between the pathological vessels and the facial nerve at the RExZ could be visualized and evaluated from various perspectives in the CPA cistern, including the simulated surgical route. The offending vessels at the RExZ of the facial nerve were as follows: AICA (five cases), PICA (four cases), PICA and VA (two cases), and AICA and vein (one case). These lesions were confirmed intraoperatively (Table 1). Alternatively, the actual site of the pathological vessels and the degree to which they compressed the facial nerve RExZ at the brainstem were assessed virtually—that is, from the viewpoint within the facial nerve directed to the nerve rootlets. The compressive sites of the offending vessels at the rootlets of the facial nerves were categorized as anterior to the nerve in 10 cases, inferior in one, and posterior in one (Table 1). The results of MVD were excellent in all patients, and symptom relief was complete immediately after surgery or in the following several days. There were no postoperative complications.

Illustrative Cases

Case 4

This 61-year-old woman underwent MVD treatment for left hemifacial spasm that had been insufficiently responsive to medical therapy for 4 years. Intraoperatively we found that the RExZ of the left facial nerve was compressed by the VA–PICA complex (Fig. 1A). Preoperative 3D MR cisternography, projected left inferolaterally and simulated through the surgical route, showed the spatial relationship of the left facial and vestibulocochlear nerves to the left VA and PICA at the RExZ (Fig. 1B). Contrast medium–enhanced 3D MR angiography (Fig. 1C), with the coregistered projection as in Fig. 1B, demonstrated the architecture of the left VA and PICA. The boundary fusion image of the 3D MR cisternogram–angiogram (Fig. 1D) depicted the pathological PICA compressing the facial nerve at the RExZ. The 3D visualization of the nerve–vessel relationship provided by the fusion images was in agreement with the intraoperative findings.

Case 9

This 54-year-old woman underwent MVD; she presented with a 5-year history of left hemifacial spasm. Intraoperatively we noted that the left facial nerve RExZ was compressed by the rostral branch of the AICA (Fig. 2A). Preoperative MR cisternography (Fig. 2B), projected superoinferiorly, showed the left AICA at the anterior aspect of the left facial nerve RExZ. A contrast agent–enhanced 3D MR angiogram (Fig. 2C) and coregistered boundary fusion image of the 3D MR cisternogram–angiogram (Fig. 2D)—viewed virtually from within the facial nerve and projected toward the rootlet at the brainstem—showed the causative site; the facial nerve rootlet was compressed by the ascending rostral branch of the AICA anterosuperiorly. On the 3D MR angiogram (Fig. 2C), the rostral branch of the AICA was not depicted continuously but was clearly identifiable, on the boundary fusion 3D MR cisternogram, as a series of rings in blue and seen transparently through the affected facial nerve (Fig. 2D). The selected minimum-intensity projection image of the preoperative MR cisternogram (Fig. 2E), projected superoinferiorly, and the 3D MR cisternogram (Fig. 2F) and boundary fusion image (Fig. 2G), projected left superiorly, demonstrated the spatial relationship of the left facial and vestibulocochlear nerves to the left AICA complex at the RExZ. The AICA diverged into the premeatal caudal and ascending rostral branches; at its origin the rostral branch ran in a hairpin-shaped course and compressed the anterosuperior aspect of the facial nerve at the RExZ. Postoperatively, the mini-

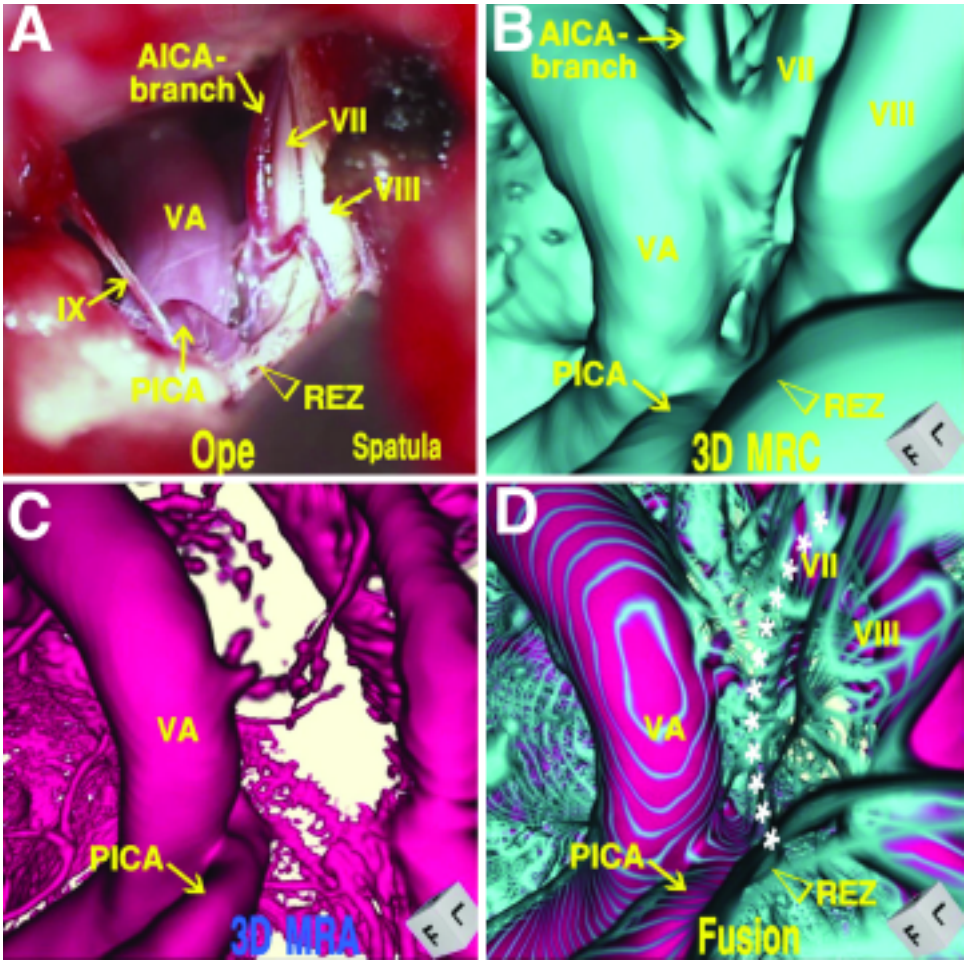

FIG. 1. Case 4. Studies obtained in a 61-year-old woman with left hemifacial spasm. A: Intraoperative photograph showing compression of the left facial nerve RExZ by the PICA–VA complex. B–D: Preoperative 3D MR cisternogram (B), 3D MR angiogram (C), and boundary fusion image of the 3D MR cisternogram–angiogram (D), projected left inferolaterally and simulated surgical route, showing the nerve–vessel relationship at the facial nerve RExZ. The *white dotted curve* in D shows the course of the facial nerve to its rootlet at the brainstem. Fusion = fused image of 3D MR angiogram–cisternogram; MRA = MR angiogram; MRC = MR cisternogram; Ope = intraoperative image; REZ = root exit zone; VII = seventh cranial nerve; VIII = eighth cranial nerve; IX = ninth cranial nerve.

mum-intensity projection image of the MR cisternogram (Fig. 2H), projected superoinferiorly, and the 3D MR cisternogram (Fig. 2I) and boundary fusion image (Fig. 2J), projected left superiorly, showed the desired separation of the pathological AICA complex from the facial nerve RExZ created by the microsurgical dissection and interposition of a prosthesis.

Case 11

This 66-year-old woman had undergone MVD for left hemifacial spasm 5 years previously, but the symptoms recurred within a year and gradually worsened. An MR cisternogram (Fig. 3A), projected superoinferiorly, showed the left PICA at the anterior aspect of the left facial nerve RExZ. The prosthesis was not observed between the offending PICA and the facial nerve RExZ, but was seen in the neighboring cistern. Intraoperatively we noted the prosthesis and the offending PICA at the facial nerve RExZ (Fig. 3B and C). The 3D MR cisternogram (Fig. 3D), 3D MR angiogram (Fig. 3E), and boundary fusion 3D MR cisternogram–angiogram (Fig. 3F), projected left superolaterally, showed that the offending PICA compressed the anterior aspect of the facial nerve RExZ and that the prosthesis was within the cistern.

Discussion

The RExZ of the facial nerve exists medially to the RExZ of the vestibulocochlear nerve within the supraolivary fossula. The supraolivary fossula is located in the lateral aspect of the pontomedullary junction—anterosuperior to the choroid plexus protruding from the foramen of Luschka; anterior to the cerebellar flocculus; rostral to a line drawn along the junction of the rootlets of the glossopharyngeal, vagus, and accessory nerves within the brainstem; and slightly posterior to the rostral pole of the inferior olivary body.[7,16] The offending vessels may be located on either the anterosuperior or anteroinferior aspect of the facial nerve at its exit from the brainstem.[7,9,10,16,19] In the most common type of hemifacial spasm that originates

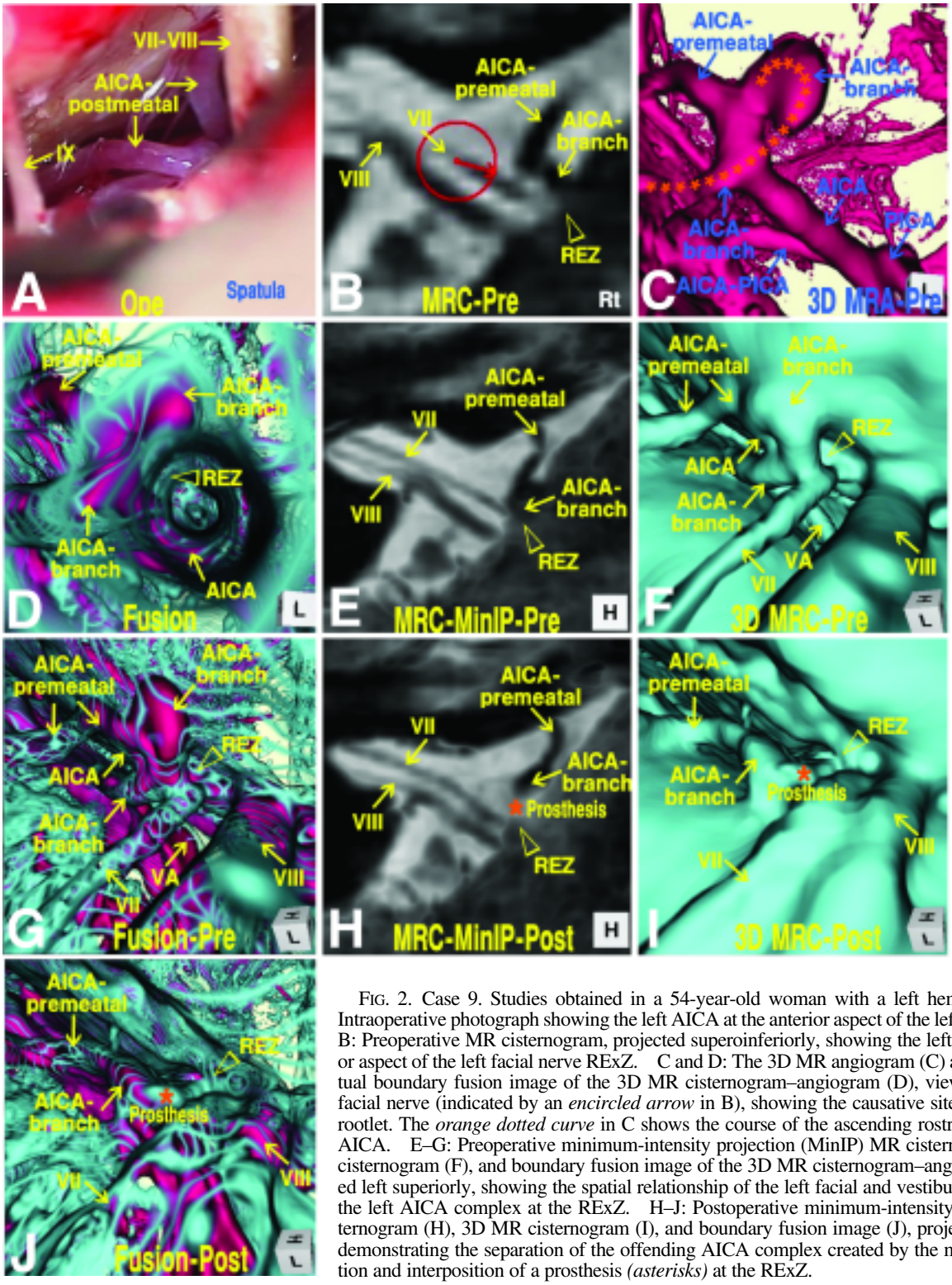

FIG. 2. Case 9. Studies obtained in a 54-year-old woman with a left hemifacial spasm. A: Intraoperative photograph showing the left AICA at the anterior aspect of the left facial nerve RExZ. B: Preoperative MR cisternogram, projected superoinferiorly, showing the left AICA at the anterior aspect of the left facial nerve RExZ. C and D: The 3D MR angiogram (C) and coregistered virtual boundary fusion image of the 3D MR cisternogram–angiogram (D), viewed from inside the facial nerve (indicated by an *encircled arrow* in B), showing the causative site on the facial nerve rootlet. The *orange dotted curve* in C shows the course of the ascending rostral branch of the left AICA. E–G: Preoperative minimum-intensity projection (MinIP) MR cisternogram (E), 3D MR cisternogram (F), and boundary fusion image of the 3D MR cisternogram–angiogram (G), projected left superiorly, showing the spatial relationship of the left facial and vestibulocochlear nerves to the left AICA complex at the RExZ. H–J: Postoperative minimum-intensity projection MR cisternogram (H), 3D MR cisternogram (I), and boundary fusion image (J), projected left superiorly, demonstrating the separation of the offending AICA complex created by the microsurgical dissection and interposition of a prosthesis *(asterisks)* at the RExZ.

in the orbicularis oculi muscle and spreads downward to involve the lower face, the anteroinferior aspect of the RExZ of the facial nerve will be compressed.[1,6] The causative vessels are pre- or postmeatal segments of the AICA and its branches, the PICA, VA, veins, and a combination of these vessels.[9,10,19]

In a procedure involving an MVD for hemifacial spasm performed via the lateral suboccipital approach, the offending vessels are mobilized and lifted away from the facial nerve RExZ; to achieve this, prosthetic material is interposed caudally through a space between the glossopharyngeal nerve and the flocculus. Because the facial nerve runs

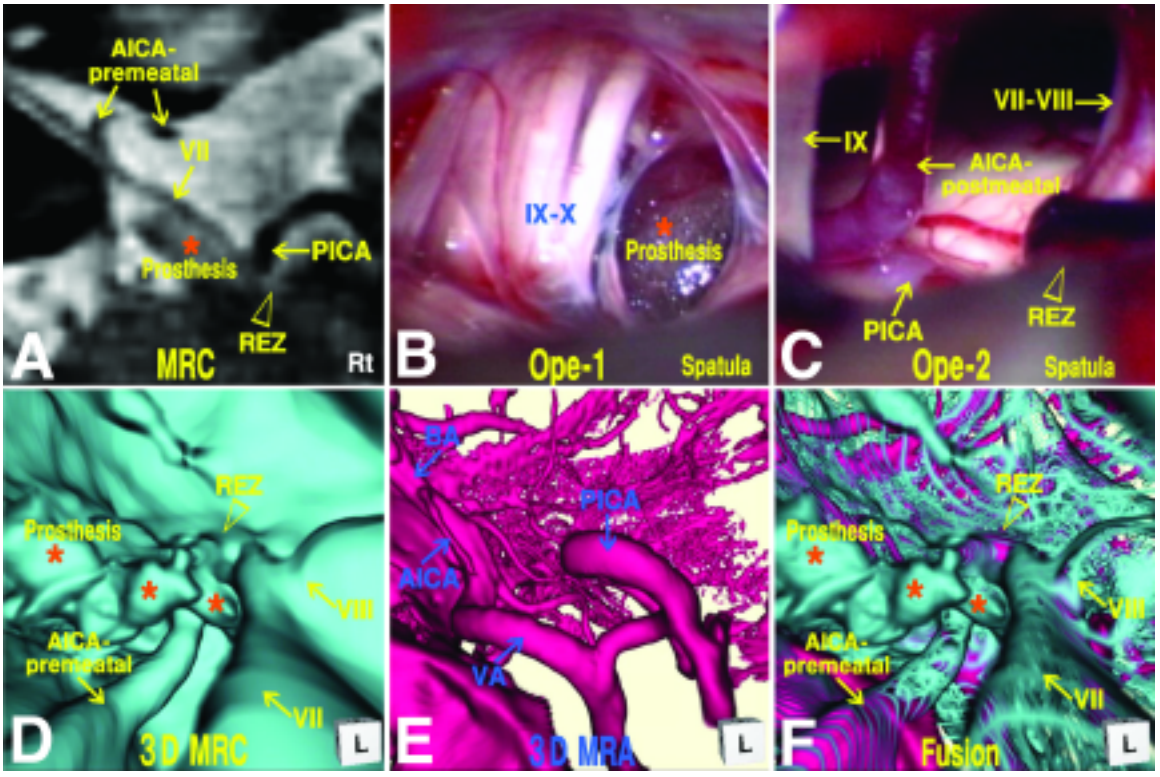

FIG. 3. Case 11. Studies obtained in a 66-year-old woman with a recurrent left hemifacial spasm. A: Preoperative MR cisternogram, projected superoinferiorly, showing the left PICA and an aberrant prosthesis *(asterisk)* at the RExZ of the left facial nerve. B and C: Intraoperative photographs demonstrating an aberrant prosthesis (*asterisk* in B) and the nerve–vessel relationship at the facial nerve RExZ (C). D–F: Preoperative 3D MR cisternogram (D), 3D MR angiogram (E), and boundary fusion image of the 3D MR cisternogram–angiogram (F), projected left superolaterally, showing direct compression of the facial nerve RExZ by the offending PICA, with scattered aberrant prosthetic material *(asterisks)* within the cistern. BA = basilar artery; X = 10th cranial nerve.

anterior to the flocculus, choroid plexus, and vestibulocochlear nerve,[7,16] one may have difficulty seeing the facial nerve directly at its junction with the brainstem. Therefore, it is important to evaluate the preoperative images for the complex nerve–vessel relationship around the facial nerve RExZ from various perspectives within the CPA cistern before initiating the actual surgical access for the MVD.

Because of recent advances in MR imaging techniques, the relationship of the anatomical elements in and around the CPA cistern can be depicted; thus, the surgeon has foreknowledge of the causative vessels in proximity to and actually compressing the facial nerve at the RExZ. With 3D TOF SPGR imaging, the cranial nerves and brain parenchyma are represented by relatively low signal intensity, and the vessels are delineated by profoundly high signal intensity (bright blood). Vessels near the RExZ of the facial nerve are clearly visualized in contrast to the surrounding facial and vestibulocochlear nerves, flocculus, choroid plexus, and brainstem. Additionally, steady-state contrast medium–enhanced MR angiograms, obtained using the 3D TOF SPGR sequence after the intravenous administration of contrast medium, can enhance the depiction of vessels with relatively slow-flow velocity, due to T_1 signal shortening effect of the intravascular paramagnetic agents.[1,8] In relation to veins and venous sinuses, small branches and distal portions of the AICA and PICA adjacent to the facial nerve are represented more clearly than those on conventional unenhanced MR angiography. The vascular structures demonstrated on 3D TOF SPGR imaging with or without contrast medium administration, however, do not indicate the luminal morphological features, as shown by digital angiography and computed tomography angiography. The MR angiogram depicts the intravascular flow condition caused by an inflow effect related mainly to the peak flow velocity of the vessels with or without a T_1 signal shortening effect.[20–23]

In contrast, MR cisternograms, obtained using constructive interference in steady state;[13,14,25] fast imaging employing steady-state acquisition, or true fast asymmetrical spin echo;[2,24] 3D FASE;[13] and 3D FSE imaging,[11,12,17,18,20–22] depict the vascular structures, cranial nerves, and brain parenchyma with low signal intensity, so that the space-occupying intra- and juxtacisternal structures are well demarcated by the hyperintense adjacent subarachnoid CSF. In particular, MR cisternograms obtained using T_2-weighted 3D FASE or 3D FSE imaging,[11–13,17,18,20–22] with fine adjustment of echo time and repetition time, can demonstrate the vascular structures as complete flow voids with profoundly low signal intensity (black blood), the cranial nerves and brain parenchyma with moderately low signal intensity, and the CSF with profoundly high signal intensity. These features may be useful to distinguish the boundary of vascular structures from the cranial nerves within the cistern in conjunction with the surrounding brain parenchyma.

The 3D anatomical relationship of the nerve–vessel structures around the facial nerve RExZ is complicated. It may be difficult to acquire a precise understanding of the spatial architecture by simply reviewing one or more of the source images displayed two dimensionally. The 3D reconstruction of the volumetric MR cisternography data (with a perspective volume-rendering algorithm) can isolate the entire area for which the signal intensity is lower than that of the CSF from the whole volume-rendering data set and can do so without targeting or trimming of the region of interest.[20–22] Consequently, the conventional 3D MR cisternogram provides an extensive spatial view of the complicated anatomical elements within a cistern, including the facial nerve, offending vessels, and surrounding brainstem.

In addition, the boundary 3D MR cisternogram, reconstructed using a perspective volume-rendering algorithm with transluminal imaging technique,[22,23] allows the imaging of boundaries. The contours of foreground objects are depicted as a series of rings, so that the underlying structures are visualized directly through the spaces between rings from outside or inside the objects. In a case in which the facial nerve RExZ is hidden by the flocculus, choroid plexus, and vestibulocochlear nerve, the boundary between the facial nerve rootlet and the brainstem can be discerned through the transparent obstacles in the foreground.

By using a fused 3D MR cisternogram–angiogram, both the nerve–vessel structures depicted on the 3D MR cisternogram and the vascular structures demonstrated on the 3D MR angiogram are coregistered in a single 3D image. With a boundary fusion 3D MR cisternogram–angiogram, the vascular components depicted on the 3D MR cisternogram can be discriminated by referencing the overlapping 3D MR angiogram. Consequently, the transparent fusion 3D MR cisternogram–angiogram can provide a precise assessment of the actual contact and compression between the offending vessels and the facial nerve RExZ. The site of neurovascular compression at the nerve rootlet from the brainstem was assessed preoperatively in 3D fashion from various viewpoints in the CPA cistern and virtually within the facial nerve.

Because the retraction of the petrosal surface of the cerebellum, choroid plexus, and flocculus and the dissection of the arachnoid membranes are usually performed during surgical manipulation, the preoperative 3D cisternograms may not be identical to the operative fields, but the shape of the anatomical elements and their spatial relationships, without surgical manipulation, correlate well with the intraoperative findings. The movement of the intra- and juxtacisternal structures following surgical exposure always compromises the comparison of the pre- and intraoperative studies.

Preoperatively, the spatial relationships between the offending vessels and the facial nerve RExZ can be assessed from various perspectives, including the simulated surgical route, and may provide useful information for the preoperative planning of the MVD. Because the offending vessels usually compress the anterior aspect of the facial nerve RExZ and because the actual compressive sites are sometimes not visible through the surgical route, virtual visualization of the compressive site of the offending vessels in relation to the entire shape of the facial nerve rootlets may be helpful before placing the prosthetic material. In our small series of patients with hemifacial spasm, we included one patient (Case 11) with recurrent hemifacial spasm. Preoperative boundary fusion 3D MR cisternography–angiography assessment clearly depicted the spatial relationship between the nerve–vessel complex and the prosthesis. The residual prosthetic material was shown to be out of place, and the facial nerve was directly compressed by an offending PICA at the facial nerve RExZ; the intraoperative findings confirmed the relationship of the nerve–vessel complex and the prosthesis. Postoperatively, a fusion image of the 3D MR cisternography–angiography study was obtained in most cases. To confirm the success of MVD in patients with hemifacial spasm, it was helpful to visualize the entire course of the dislocated offending vessels—now no longer compressing the facial nerve—and the interposition of the prosthesis.

Consequently, the fused 3D MR cisternography–angiography imaging technique may prove useful as a preoperative adjunct and also in the postoperative assessment of MVD in patients with hemifacial spasm. The fusion imaging modality may provide helpful information regarding the neurovascular conflict at the time of MVD in patients with typical hemifacial spasm. In particular, it may be valuable in demonstrating a misplaced prosthesis when assessing patients with recurrent spasms. The significance of these imaging findings, however, needs to be clarified in a larger population, including one in which there are false-negative and false-positive results. Additionally, it is necessary to obtain a more precise image of the compressive site and the degree of the offending vessels, in conjunction with fine arterioles, perforating structures, and small veins around the facial nerve RExZ. More work is required to validate the imaging technique and clarify the accuracy of the pathological neurovascular conflict in patients with hemifacial spasm.

Conclusions

Coregistered fusion images of 3D MR cisternograms and 3D MR angiograms may be useful in the pre- and postoperative assessment of MVD in patients with hemifacial spasm. The complex nerve–vessel structures at the RExZ of the facial nerve can be visualized three dimensionally. The relationship between the offending vessels and the facial nerve at the rootlets of the brainstem may be discerned preoperatively and seen from various perspectives within the CPA cistern, within the facial nerve, and through the simulated surgical route. The 3D visualization of the nerve–vessel relationship obtained using the present technique was comparable to the intraoperative findings. Postoperatively, the success of the microsurgical dissection and interposed prosthesis in relation to the pathological vessels can be confirmed on a fusion image. In this light, the 3D MR cisternogram–angiogram fusion technique can be applied to investigate other neurovascular compressive syndromes including trigeminal neuralgia,[1,2,14,24,25] glossopharyngeal neuralgia,[5,14] vestibulocochlear compressive tinnitus and hearing loss,[4,15] and neurogenic hypertension.[3,14]

Acknowledgments

We thank Miss Megumi Omi, radiological technologist, of Ryofukai Satoh Neurosurgical Hospital, for her technical assistance in conducting the MR imaging studies.

References

1. Boecher-Schwarz HG, Bruehl K, Kessel G, Guenthner M,

Perneczky A, Stoeter P: Sensitivity and specificity of MRA in the diagnosis of neurovascular compression in patients with trigeminal neuralgia. A correlation of MRA and surgical findings. **Neuroradiology 40:**88–95, 1998
2. Chávez GD, De Salles AAF, Solberg TD, Pedroso A, Espinoza D, Villablanca P: Three-dimensional fast imaging employing steady-state acquisition magnetic resonance imaging for stereotactic radiosurgery of trigeminal neuralgia. **Neurosurgery 56:** E628, 2005
3. Colón GP, Quint DJ, Dickinson LD, Brunberg JA, Jamerson KA, Hoff JT, et al: Magnetic resonance evaluation of ventrolateral medullary compression in essential hypertension. **J Neurosurg 88:**226–231, 1998
4. De Ridder D, Ryu H, Møller AR, Nowé V, Van de Heyning P, Verlooy J: Functional anatomy of the human cochlear nerve and its role in microvascular decompressions for tinnitus. **Neurosurgery 54:**381–390, 2004
5. Fischbach F, Lehmann TN, Ricke J, Bruhn H: Vascular compression in glossopharyngeal neuralgia: demonstration by high-resolution MRI at 3 tesla. **Neuroradiology 45:**810–811, 2003
6. Girard N, Poncet M, Caces F, Tallon Y, Chays A, Martin-Bouyer P, et al: Three-dimensional MRI of hemifacial spasm with surgical correlation. **Neuroradiology 39:**46–51, 1997
7. Hitotsumatsu T, Matsushima T, Inoue T: Microvascular decompression for treatment of trigeminal neuralgia, hemifacial spasm, and glossopharyngeal neuralgia: three surgical approach variations: technical note. **Neurosurgery 53:**1436–1443, 2003
8. Jäger HR, Ellamushi H, Moore EA, Grieve JP, Kitchen ND, Taylor WJ: Contrast-enhanced MR angiography of intracranial giant aneurysms. **AJNR Am J Neuroradiol 21:**1900–1907, 2000
9. Jannetta PJ, Abbasy M, Maroon JC, Ramos FM, Albin MS: Etiology and definitive microsurgical treatment of hemifacial spasm. Operative techniques and results in 47 patients. **J Neurosurg 47:**321–328, 1977
10. Kondo A: Follow-up results of microvascular decompression in trigeminal neuralgia and hemifacial spasm. **Neurosurgery 40:** 46–52, 1997
11. Mamata Y, Muro I, Matsumae M, Komiya T, Toyama H, Tsugane R, et al: Magnetic resonance cisternography for visualization of intracisternal fine structures. **J Neurosurg 88:**670–678, 1998
12. Mitsuoka H, Tsunoda A, Okuda O, Sato K, Makita J: Delineation of small nerves and blood vessels with three-dimensional fast spin-echo MR imaging: comparison of presurgical and surgical findings in patients with hemifacial spasm. **AJNR Am J Neuroradiol 19:**1823–1829, 1998
13. Naganawa S, Koshikawa T, Fukatsu H, Ishigaki T, Fukuta T: MR cisternography of the cerebellopontine angle: comparison of three-dimensional fast asymmetrical spin-echo and three-dimensional constructive interference in the steady-state sequences. **AJNR Am J Neuroradiol 22:**1179–1185, 2001
14. Naraghi R, Hastreiter P, Tomandl B, Bonk A, Huk W, Fahlbusch R: Three-dimensional visualization of neurovascular relationships in the posterior fossa: technique and clinical application. **J Neurosurg 100:**1025–1035, 2004
15. Okamura T, Kurokawa Y, Ikeda N, Abiko S, Ideguchi M, Watanabe K, et al: Microvascular decompression for cochlear symptoms. **J Neurosurg 93:**421–426, 2000
16. Rhoton AL Jr: The cerebellopontine angle and posterior fossa cranial nerves by the retrosigmoid approach. **Neurosurgery 47 (3 Suppl):**S93–S129, 2000
17. Rubinstein D, Sandberg EJ, Breeze RE, Sheppard SK, Perkins TG, Cajade-Law AG, et al: T2-weighted three-dimensional turbo spin-echo MR of intracranial aneurysms. **AJNR Am J Neuroradiol 18:**1939–1943, 1997
18. Ryu H, Tanaka T, Yamamoto S, Uemura K, Takehara Y, Isoda H: Magnetic resonance cisternography used to determine precise topography of the facial nerve and three components of the eighth cranial nerve in the internal auditory canal and cerebellopontine cistern. **J Neurosurg 90:**624–634, 1999
19. Samii M, Günther T, Iaconetta G, Muehling M, Vorkapic P, Samii A: Microvascular decompression to treat hemifacial spasm: long-term results for a consecutive series of 143 patients. **Neurosurgery 50:**712–719, 2002
20. Satoh T, Omi M, Ohsako C, Fujiwara K, Tsuno K, Sasahara W, et al: Differential diagnosis of the infundibular dilation and aneurysm of internal carotid artery: assessment with fusion imaging of 3D MR cisternography/angiography. **AJNR Am J Neuroradiol 27:**306–312, 2006
21. Satoh T, Omi M, Ohsako C, Katsumata A, Yoshimoto Y, Tsuchimoto S, et al: Influence of perianeurysmal environment on the deformation and bleb formation of the unruptured cerebral aneurysm: assessment with fusion imaging of 3D MR cisternography and 3D MR angiography. **AJNR Am J Neuroradiol 26:** 2010–2018, 2005
22. Satoh T, Omi M, Ohsako C, Katsumata A, Yoshimoto Y, Tsuchimoto S, et al: Visualization of aneurysmal contours and perianeurysmal environment with conventional and transparent 3D MR cisternography. **AJNR Am J Neuroradiol 26:**313–318, 2005
23. Satoh T, Onoda K, Tsuchimoto S: Visualization of intraaneurysmal flow patterns with transluminal flow images of 3D MR angiograms in conjunction with aneurysmal configurations. **AJNR Am J Neuroradiol 24:**1436–1445, 2003
24. Tsuchiya K, Aoki C, Hachiya J: Evaluation of MR cisternography of the cerebellopontine angle using a balanced fast-field-echo sequence: preliminary findings. **Eur Radiol 14:**239–242, 2004
25. Yoshino N, Akimoto H, Yamada I, Nagaoka T, Tetsumura A, Kurabayashi T, et al: Trigeminal neuralgia: evaluation of neuralgic manifestation and site of neurovascular compression with 3D CISS MR imaging and MR angiography. **Radiology 228:** 539–545, 2003

Manuscript received January 4, 2006.
Accepted in final form June 27, 2006.
Presented in part at the 64th Annual Meeting of the Neurosurgical Society, October 5 to 7, 2005, Yokohama, and the 15th Japanese Congress for Computer in Neurosurgery, January 28, 2006, Yamaguchi, Japan.

Address reprint requests to: Toru Satoh, M.D., Department of Neurological Surgery, Ryofukai Satoh Neurosurgical Hospital, Fukuyama, Hiroshima 729-0104, Japan. email: ucsfbtrc@urban.ne.jp.